analytical chemistry

Article

pubs.acs.org/ac

Interfacial Micropore Defect Formation in PEDOT:PSS-Si Hybrid Solar Cells Probed by TOF-SIMS 3D Chemical Imaging

Joseph P. Thomas, Liyan Zhao, Marwa Abd-Ellah, Nina F. Heinig, and K. T. Leung*

WATLab and Department of Chemistry, University of Waterloo, Waterloo, Ontario N2L 3G1 Canada

Supporting Information

ABSTRACT: Conducting p-type polymer layers on n-type Si have been widely studied for the fabrication of cost-effective hybrid solar cells. In this work, time-of-flight secondary ion mass spectrometry (TOF-SIMS) is used to provide three-dimensional chemical imaging of the interface between poly(3,4-ethylene-dioxythiophene):polystyrenesulfonate (PEDOT:PSS) and SiO_x/Si in a hybrid solar cell. To minimize structural damage to the polymer layer, an Ar cluster sputtering source is used for depth profiling. The present result shows the formation of micropore defects in the interface region of the PEDOT:PSS layer on the SiO_x/Si substrate. This interfacial micropore defect formation becomes more prominent with increasing thickness of the native oxide layer, which is a key device parameter that greatly affects the hybrid solar cell performance. Three-dimensional chemical imaging coupled with Ar cluster ion sputtering has therefore been demonstrated as an emerging technique for probing the interface of this and other polymer−inorganic systems.

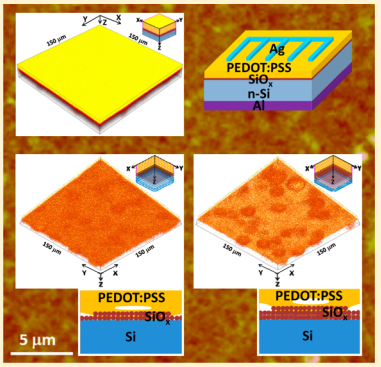

Hybrid solar cells comprised of a p-type conducting poly(3,4-ethylene-dioxythiophene):polystyrenesulfonate (PEDOT:PSS) thin film and a planar or surface-structured n-type Si substrate have been extensively investigated in the recent development of highly efficient and cost-effective solar cells.[1−6] To date, a power conversion efficiency (PCE) as high as 10−11% has been reported for this type of hybrid solar cells.[1−4] However, there have been some notable reports of PCE below 1% from the same type of solar cells.[5−7] The quality of the interface between PEDOT:PSS and Si is believed to contribute greatly to the large discrepancy observed in the PCE. Recently, Zhang et al.[8] and He et al.[2] independently concluded that a thin native SiO_x layer could be used to significantly enhance solar cell properties when compared to cells with just a H-terminated Si (H−Si) surface.[2,8] This is because the native SiO_x layer provides the crucial intermediate region in the p−i−n junction, leading to favorable internal electric fields at the interface that enhances the solar cell properties.[2] This thin native SiO_x layer can be easily formed prior to the PEDOT:PSS layer coating simply by exposing the clean Si substrate to ambient atmosphere for a few hours after the H-termination step. The thickness of the SiO_x layer is important and cannot be too large, because a thick oxide layer could create an insulating barrier for electrical transport, thereby reducing the solar cell performance. On the other hand, the hydrophilic nature of the oxide layer can improve the wettability of the aqueous dispersion of PEDOT:PSS on Si.[1,2] It has been proposed that the formation of defects at the interface could greatly affect the properties of these hybrid solar cells.[2,3] The nature of the SiO_x layer, its effects on the PEDOT:PSS/Si interface, and the nature of interfacial defect formation could all influence the solar cell properties, and to date their effects have not been fully understood.

In order to improve the wettability and to form a uniform layer of PEDOT:PSS on a Si substrate, addition of a suitable surfactant or chemical is often mandatory prior to the spin-coating process.[2,3,9−11] High-efficiency solar cells fabricated with PEDOT:PSS treated with nonionic surfactants[2,10] or a fluorosurfactant[3] on a planar Si substrate have been recently reported. Improvement in the conductivity of PEDOT:PSS with the addition of an anionic[12] or a cationic[13] surfactant has also been obtained. However, the effects of adding different surfactants to PEDOT:PSS on the solar cell properties have yet to be explored. In effect, the SiO_x layer thickness (which contributes to the interfacial electrical barrier), the conductivity and wettability of PEDOT:PSS, the spin speed and time used in spin-coating to regulate the thickness of PEDOT:PSS layer on Si, and the annealing temperature after the spin-coating process could all influence the interfacial properties of the hybrid solar cells. Detailed investigation is required to characterize the contribution from each of these factors and their roles in the interfacial properties between PEDOT:PSS and the SiO_x layer. A better understanding of these effects can provide insight into the large discrepancy in the reported PCE, and help to develop new fabrication protocols for hybrid solar cells with a high PCE.

To date, investigation of the interface by cross-sectional electron microscopic techniques is largely limited by localized two-dimensional (morphological) views of the interface, which generally lack the crucial chemical information. In contrast, a three-dimensional view of the interface can provide new insight into the nature of defects and the effects of the oxide layer at

Received: April 13, 2013
Accepted: June 6, 2013
Published: June 7, 2013

   dx.doi.org/10.1021/ac401084x | *Anal. Chem.* 2013, 85, 6840−6845

the PEDOT:PSS/SiO_x/Si junction. The capability of obtaining 3D chemical images of bulk materials using depth-profiling time-of-flight (TOF) secondary ion mass spectrometry (SIMS) has attracted much recent interest for probing in-depth information of diverse materials.[14−18] In a static SIMS experiment, a focused ion beam with doses below the static limit (10^{13} ions/cm^2) is directed onto a solid sample surface, and the emitted secondary ions are analyzed.[19,20] Along with the primary ion beam, a second ion beam of choice is used to sputter away the sample, preferably by conserving the molecular fragments in the polymer layer and with minimal material intermixing in the analysis region.[20−22] While the technique has been relatively well developed for depth profiling of hard materials, obtaining information from soft (organic or polymer) materials remains challenging mainly because of the low secondary ion yield.[20,22] With conventional sputtering ion sources (Cs or O_2), depth profiling of soft material is further complicated by the intense damage cascades generated by the sputtering ions that disrupt the original structure.[22,23] With the incorporation of a C_{60} sputtering source into the TOF-SIMS technique, the ion yields from polymer or organic materials have been improved.[20,24−28] Recently, the use of an Ar cluster ion source has been introduced and consistently found to be an even better sputtering source for organic or polymer materials in providing depth-profile information without disrupting the soft materials of interest.[20,26−29] However, this technique is still in its infancy, and further efforts are needed to exploit its advantages for organic or polymer depth-profiling experiments. 3D imaging is achieved by interleaving the analysis and sputtering cycles with the appropriate ion sources, and the resulting sequence of 2D secondary ion images are then appropriately stacked to regenerate the chemical image cube. Although the lateral resolution is currently in the submicrometer range for this SIMS technique,[21] depth resolution as high as 2.5 nm can be achieved for organic materials by using the Ar cluster source.[27] This type of 3D material characterization at high depth resolution is not possible even in advanced dual-beam scanning electron microscopy (the so-called slice-and-view technique).[30] In this report, the unique capability of TOF-SIMS, coupled with the new Ar cluster sputtering source technology, is exploited to provide 3D chemical imaging of the interfacial properties of hybrid solar cells.

Here, we elucidate the interface between PEDOT:PSS and the planar Si substrate in a hybrid solar cell by using 3D chemical imaging by TOF-SIMS. By using the Bi cluster ion source for analysis and the Ar cluster ion source for sputtering, we obtain, for the first time, 3D chemical information about the technologically important conducting polymer material, PEDOT:PSS, that has been widely used for the development of hybrid solar cells. The 3D chemical images reveal micropore defects at the PEDOT:PSS/SiO_x/Si interface. Remarkably, these defects are more apparent with increasing thickness of the native oxide layer. Native oxide layers naturally grown in air for 1 and 3 h on the H−Si substrate are found to exhibit the highest PCE, and their similar 3D chemical images both show relatively low micropore defect densities. This is in marked contrast to the poor solar cell performance and the more extended micropore defects found for a Si substrate with a thick native oxide layer.

EXPERIMENTAL SECTION

One-side-polished, n-type Si(100) substrates, with resistivity of 1−10 Ohm-cm and thickness of 300 μm (Virginia Semiconductor Inc.), were RCA-cleaned and H-terminated by immersing in 2% hydrofluoric acid for 10 min. Al metal (250 nm thick) was deposited on the unpolished side of the Si substrate in a dual-target magnetron sputtering system (EMS575X) immediately after the H-termination. Subsequently (approximately 45 min after H-termination), the substrate was allowed to stay in an ambient air atmosphere for different amounts of time (0, 1, 3, and 5 h) to facilitate formation of a naturally grown SiO_x layer (with different thicknesses). PEDOT:PSS with a dispersion content of 1.3% in water (Sigma Aldrich) was mixed with 5 wt % of dimethyl sulfoxide (DMSO) and then filtered using a 0.45 μm syringe filter. To improve the wettability of PEDOT:PSS on Si, 0.5 wt % of nonionic surfactant Triton X-100 was added prior to spin-coating. The PEDOT:PSS layer on Si was coated at a spin rate of 6000 rpm for 1 min and annealed on a hot plate at 110 °C for 10 min in air. For the top electrode, a finger-type Ag metal grid with a finger width of ∼300 μm and thickness of 50 nm was sputter-deposited on the polymer layer through a shadow mask. The fabricated solar cell samples were designated according to the SiO_x growth time (0, 1, 3, and 5 h) as Samples A, B, C, and D, respectively. As a reference, we also fabricated a solar cell using RCA-cleaned Si without H-termination and with its as-received native SiO_x layer intact (designated as Sample R).

The solar cell properties were measured using an $I-V$ measurement system (PV Measurements IV5) under 100 mW/cm^2 illumination using a class ABA solar simulator (AM 1.5G) in air. The intensity of the light source was calibrated using a Si reference cell (PVM782 with a BK7 window). The measured device area was 5 × 5 mm^2. TOF-SIMS measurement was carried out in an ION-TOF 5 system (IONTOF GmbH), equipped with a 2 m long reflectron TOF analyzer operated in the negative polarity mode, and a Bi_3^+ ion analysis beam source and an Ar cluster ion (Ar_{1000}^+) sputtering beam source. Depth profiling was carried out in the spectrometry mode (non-interlaced) with an analysis ion beam current of 0.8 pA, a cycle time of 200 μs, and a sampling area of 150 × 150 μm^2 (256 × 256 pixels). Sputtering was carried out with Ar cluster ions at an ion beam energy of 5 keV and with an ion current of 1.8 nA over an area of 400 × 400 μm^2. The TOF-SIMS spectra (Supporting Information, Figure S1) were mass-calibrated on C_x fragments. The surface morphology and roughness of the samples were examined by tapping-mode atomic force microscopy (AFM) in a Digital Instruments Dimension 3100 Nanoscope IV. The oxide layer thickness of the RCA-cleaned Si substrate was estimated by using reflectometry (Filmetrics F40-UV).

RESULTS AND DISCUSSION

The current density−voltage ($J-V$) curves for PEDOT:PSS/planar-Si hybrid solar cells fabricated (after appropriate backside Al deposition) on H−Si followed by exposure to air for 0−5 h (Samples A−D) are shown in Figure 1. A reference cell on RCA-cleaned Si (without H-termination) is also fabricated, and its $J-V$ curve (Sample R) is also shown in Figure 1. The inset shows a schematic diagram of the PEDOT:PSS/SiO_x/Si device structure. The photovoltaic properties of Samples A−D and R are summarized in Table

dx.doi.org/10.1021/ac401084x | Anal. Chem. 2013, 85, 6840−6845

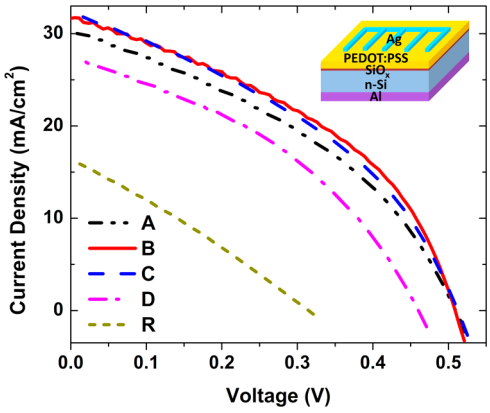

Figure 1. Current density vs voltage ($J-V$) curves for the PEDOT:PSS/planar-Si hybrid solar cells fabricated with the H-terminated Si substrate exposed to air for (A) 0, (B) 1, (C) 3, and (D) 5 h followed by appropriate backside Al deposition. Curve R shows the $J-V$ data for a reference solar cell fabricated on RCA-cleaned Si substrate with its native oxide intact (i.e., without H-termination). The inset shows schematically the device structure of the hybrid solar cell.

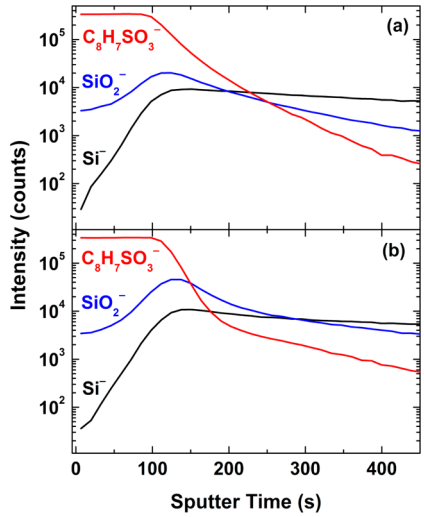

Figure 2. Depth-profiles of $C_8H_7SO_3^-$, SiO_2^-, and Si^- ions for PEDOT:PSS layers spin-coated on (a) H-terminated Si substrate exposed to air for 1 h (Sample B), and (b) RCA-cleaned Si substrate with its native oxide intact (without H-termination, Sample R).

1. A PCE of 4.53% is achieved for the solar cell fabricated on H−Si without any postexposure to air (Sample A). The PCE is found to increase to 5.08% and then decrease slightly to 4.89% for the cells with H−Si exposed to air for 1 h (Sample B) and 3 h (Sample C), respectively. However, the PCE for the cell fabricated with H−Si exposed to air for 5 h (Sample D) is markedly reduced to 3.72%. The reference cell (Sample R) is found to have a significantly lower PCE of just 1.10% (Table 1). The short-circuit current density, J_{sc}, increases from 23.2 (Sample A) to 24.3 (Sample B) and 24.4 mA/cm^2 (Sample C) and then decreases to 20.7 mA/cm^2 (Sample D). The open-circuit potential, V_{oc} (0.51 V), is found to be the same for Samples A−C but reduced to 0.46 V for Sample D. A fill factor (FF) of 41.2% is obtained from Sample B that is higher than those of Samples A (38.4%), C (39.2%), and D (39.1%). For Sample R, J_{sc} of 12.5 mA/cm^2, V_{oc} of 0.31 V, and FF of 28% are obtained. It is clear that a SiO_x layer with an appropriate thickness, such as that obtained by air exposure for 1−3 h, is essential to achieving better solar cell performance. However, a SiO_x layer that is too thick can be detrimental to the solar cell performance because the presence of a larger interfacial barrier reduces charge transport and increases series resistance.[2]

To investigate the interfacial characteristics that affect the properties of our solar cells, we carry out TOF-SIMS depth-profiling studies and construct 3D chemical images of their interfaces. The depth-profiles obtained for Sample B (PEDOT:PSS/H−Si with 1 h air exposure) are shown in Figure 2a. We have chosen the $C_8H_7SO_3^-$ ion as the marker for identifying the PEDOT:PSS component, while SiO_2^- and Si^- ions are used for the interfacial oxide and Si substrate components, respectively. As a reference, we show in Figure 2b the corresponding depth-profiles of the PEDOT:PSS layer on the native SiO_x/Si substrate in our reference cell (Sample R). The depth-profile data (Figure 2a) shows that sputtering for ∼100 s is required to reach the interface between PEDOT:PSS and SiO_x. The sputtering rate of the PEDOT:PSS layer (70 nm thick) using the Ar cluster ions is estimated to be 1.4 nm/s by profilometry and independently verified by cross-sectional scanning electron microscopy measurement. The PEDOT:PSS profile crosses that of Si at 220 s sputtering time, which marks the interfacial region with the onset of diffusion of PEDOT:PSS to Si through the thin SiO_x layer (Figure 2a). The SiO_x layer is expected to be less than 2 nm thick on the H−Si substrate with 1 h air exposure,[2] which is consistent with the small peak observed after sputtering for 100−125 s. The SiO_x profile is found to intersect the Si profile at 200 s sputtering time. Similar depth-profiles have also been obtained for other samples (A, C, and D). For the reference sample (Sample R, Figure 2b), the broader and more intense peak in the corresponding SiO_2^- depth-profile shows a thicker native oxide layer (above 2 nm),[2] as indicated by the crossing of the SiO_2^- profile with the Si^- profile at a higher sputtering time of 250 s. As shown by the more rapid drop-off in the $C_8H_7SO_3^-$ profile (i.e., over a shorter range of sputtering time), the thicker oxide layer evidently restricts the diffusion of PEDOT:PSS to the Si substrate. The smaller overall magnitudes of the SiO_2^- and Si^- depth-profiles also reflect the characteristic low sputtering rates of the Ar cluster ions for oxide or inorganic materials.

Table 1. Photovoltaic Properties of PEDOT:PSS/Planar-Si Hybrid Solar Cells

cell sample	SiO_x growth time (h) [after H-termination]	J_{SC} (mA/cm^2)	V_{OC} (V)	FF (%)	PCE (%)
A	0	23.2	0.51	38.4	4.53
B	1	24.3	0.51	41.2	5.08
C	3	24.4	0.51	39.2	4.89
D	5	20.7	0.46	39.1	3.72
R	native SiO_x[a]	12.5	0.31	28.0	1.10

[a]RCA-cleaned Si substrate without H-termination.

dx.doi.org/10.1021/ac401084x | Anal. Chem. 2013, 85, 6840−6845

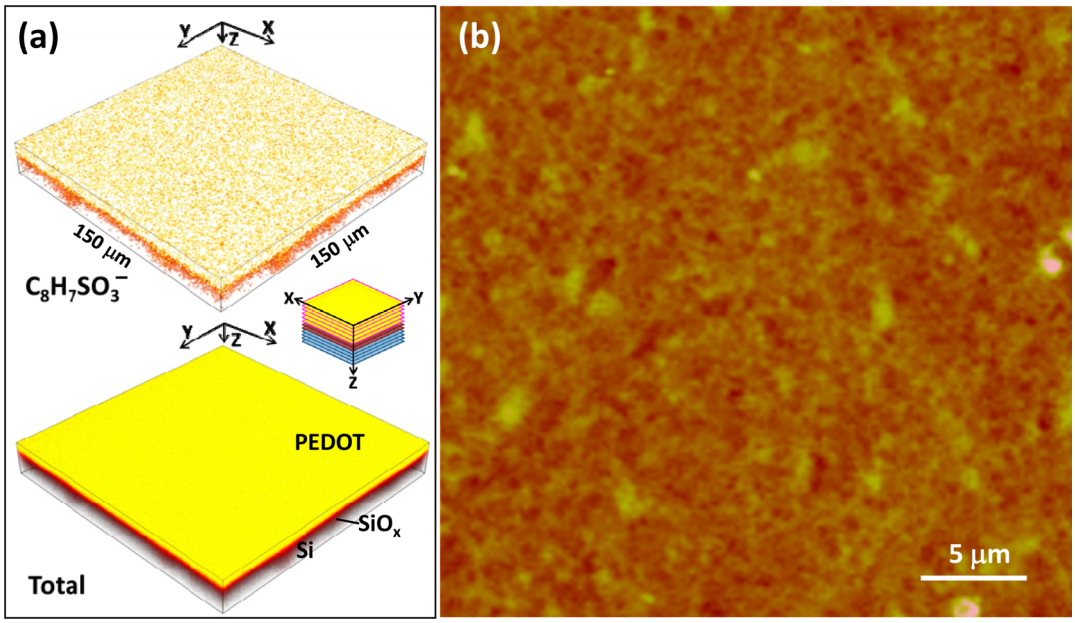

Figure 3. Top perspective views of 3D TOF-SIMS images of (a) $C_8H_7SO_3^-$ and total ions, and (b) AFM image (z scale of 0−86 nm) for a typical area (30 × 30 μm^2) of a PEDOT:PSS layer spin-coated on a H-terminated Si substrate exposed to air for 1 h (Sample B). The inset in (a) shows a schematic diagram of the stack of 2D ion maps used to reconstruct the 3D chemical image cube (150 × 150 × 0.73 μm^3).

We show in Figure 3a the top perspective views of the corresponding 3D images for the $C_8H_7SO_3^-$ ion and total ions over a typical analysis area (150 × 150 μm^2) for Sample B. The total ion image corresponds to the sum of $C_8H_7SO_3^-$, SiO_2^-, and Si^- ion images. These three-dimensional (3D) (*XYZ*) chemical images are reconstructed by stacking, along the depth direction (*Z*), 2D (*XY*) maps obtained interleavingly between sputtering cycles. A schematic diagram of the construction of the 3D SIMS image is also shown in the figure. Evidently, a smooth topmost surface is observed from the images, which is in good agreement with the corresponding AFM image of the topmost surface of PEDOT:PSS layer shown in Figure 3b. A surface roughness (rms) of 13 nm is estimated from the AFM image. The interfacial information can be revealed by examining the bottom perspective views of the 3D images shown in Figure 4a, obtained by rotating the top perspective view by 180° on the *Z* axis. Remarkably, the bottom perspective views of the 3D chemical images for the $C_8H_7SO_3^-$ ions show the presence of micropores at the interface. The appearance of these structures is much more prominent for the PEDOT:PSS layer on the thick native SiO_x/Si substrate (Sample R, Figure 4b). It is also apparent that the as-formed micropores are randomly distributed at the interface.

Figure 5 shows the 2D *XY* bottom view of the $C_8H_7SO_3^-$ 3D ion image cube for the same sample B, which corresponds to the stacks of scan data projected along the *Z* direction (from the interface to the topmost surface). The micropore structures are found to be approximately 16 μm in average diameter. In order to examine the origin and nature of these structures, we reconstruct cross-sectional *XZ* and *YZ* views of a selected micropore (Area P). The two cross sections show that the micropore extends into the Si substrate through the SiO_x layer. Furthermore, the corresponding depth-profiles of $C_8H_7SO_3^-$, SiO_2^-, and Si^- regenerated from Area P (16 × 16 μm^2) and from a nearby *XY* area without any micropore of identical size (Area Q) show that the PEDOT:PSS-SiO_x interface is reached after sputtering for 100−110 s. The 10-s span in the sputtering time can be attributed to the surface roughness of the PEDOT:PSS layer. For Area Q, the PEDOT:PSS component is completely removed after sputtering for 300 s. However, for Area P, this component starts to diminish at the PEDOT:PSS-SiO_x interface (after sputtering for 110 s), and remains discernible even after the oxide layer has been removed by sputtering for 440 s. This more gradual reduction indicates diffusion of PEDOT:PSS to Si through the thin oxide layer. The shaded part in the depth-profiles of Area P marks a hollow region along the depth direction inside the micropore structure near the interface of the PEDOT:PSS layer. The weak broad feature in the 300−400 s region in the PEDOT:PSS profile for Area P further supports the presence of the hollow region inside the PEDOT:PSS layer. In addition, the slightly different sputtering times to reach the interface between the oxide and Si for Area P (125 s) and Area Q (85 s) indicate nonuniformity in the oxide layer thickness. Furthermore, to investigate the effect of impurities, such as Na or polydimethylsiloxane (PDMS), on the formation of micropores, we carry out depth-profiling analysis in the positive ion mode. The positive ion images for Na^+ and PDMS (m/z = 147) do not exhibit any micropore feature at the interface, which indicates that these impurities do not contribute to the observed formation of micropores.

The origin of this micropore formation is not completely clear. It is apparent that the nonuniform oxide layer interacts with PEDOT:PSS and particle sedimentation increases with increasing thickness of the oxide layer at the interface, which could lead to micropore formation at the interface. A thinner oxide layer (Samples A−D) is not expected to restrict the diffusion of PEDOT:PSS to the Si substrate, which is consistent with our results that the diffusion is extended to the Si substrate. On the other hand, a thicker native oxide layer (5.5 ± 1 nm, Sample R) is found to limit the diffusion of PEDOT:PSS to Si through the SiO_x (Supporting Information, Figure S2), which could enhance sedimentation of the polymer due to its higher wettability. Since the sputtering efficiency using the Ar cluster ions for the oxide layer is much lower than that for

dx.doi.org/10.1021/ac401084x | *Anal. Chem.* 2013, 85, 6840−6845

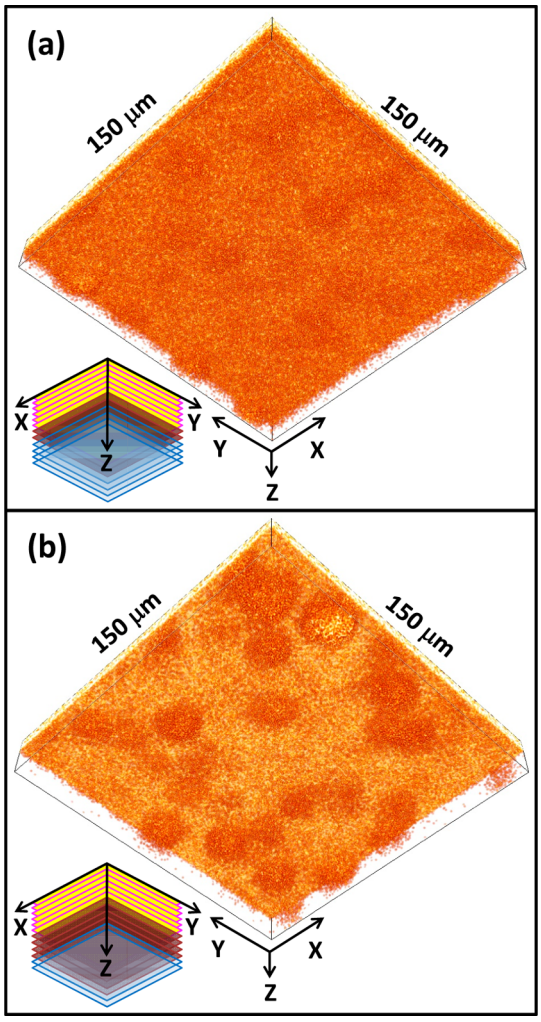

Figure 4. Bottom perspective views of 3D TOF-SIMS images of $C_8H_7SO_3^-$ ions (obtained after 35 scans interleaved with Ar_{1000} cluster ion beam sputter cycle) of PEDOT:PSS layers spin-coated on (a) a H-terminated Si substrate exposed to air for 1 h (Sample B) and (b) RCA-cleaned Si substrate with a native oxide layer (Sample R). The insets in (a) and (b) show schematic diagrams of the stacks of 2D ion maps used to reconstruct the respective 3D chemical image cubes (150 × 150 × 0.73 μm^3).

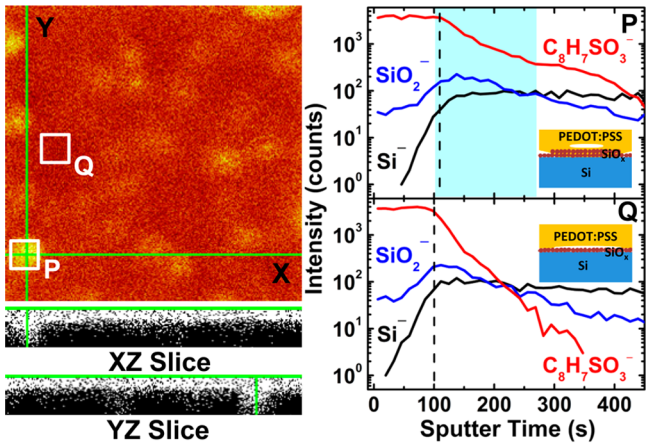

Figure 5. Bottom view of 3D TOF-SIMS image of $C_8H_7SO_3^-$ ion (150 × 150 μm^2) of a PEDOT:PSS layer spin-coated on a H-terminated Si substrate exposed to air for 1 h (Sample B). The two bottom left panels show *XZ* and *YZ* cross-sectional planes obtained along the respective green lines. The yellow color in the 2D image and the white color in the cross sections correspond to a higher molecular signal. The depth-profiles for $C_8H_7SO_3^-$, SiO_2^-, and Si^- ions obtained from selected areas (16 × 16 μm^2) of the image at P and Q are shown in the right panels. The dotted lines mark the interfacial regions between the PEDOT:PSS layer and the SiO_x/Si substrate, and the shaded area highlights the depression in the depth-profile caused by the micropore. The insets show the respective schematic illustrations of possible micropore formation at the interfaces for Areas P and Q.

PEDOT:PSS, the corresponding sputtering rates could be affected in the PEDOT:PSS diffused oxide region, consistent with the more extended depth-profile of the PEDOT:PSS component over a longer sputtering time for Area P (shown in Figure 5). Further sputtering times needed to completely remove PEDOT:PSS from Area P and Area Q indicates that the micropore formation occurs near 55 nm beneath the topmost surface and the micropore height (void thickness) is estimated to be less than 10 nm. Schematic illustrations of possible micropore formation at the interfaces of the hybrid solar cells are shown as insets in Figure 5. A similar result is also observed from the analysis of Sample R (Supporting Information, Figure S2), which indicates the presence of micropores with a similar diameter but apparently slightly larger micropore height. A thin oxide layer at the interface could promote upward band bending of Si, thereby enhancing carrier separation and carrier recombination at the interface.[2] On the other hand, a thicker oxide layer could introduce a charge transport barrier, which increases the series resistance that diminishes the solar cell properties. It is clear that a thin oxide layer formed in 1−3 h (corresponding to 1.5−2.2 nm film thickness,[2] Samples B and C) has apparently created internal electric field configuration that leads to better performance in hybrid solar cells. The thin oxide layer can enhance the wettability and limit the formation of micropores at the interface between PEDOT:PSS and Si with small micropore heights. On the other hand, increasing the thickness of the oxide layer at the interface produces larger micropore heights, adding to the interfacial electrical resistance that reduces the solar cell performance. Optimizing the formation of the PEDOT:PSS layer with less micropore formation by using a thin uniform oxide layer could therefore provide better solar cell performance.

■ CONCLUSIONS

The hybrid solar cell interface has been investigated by TOF-SIMS 3D chemical imaging employing Ar cluster ions for material sputtering. The present study definitively shows the formation of micropore defects at the PEDOT:PSS/SiO_x/Si interface, which could adversely influence the hybrid solar cell properties. The formation of these micropores at the interface is found to be greatly affected by the native oxide layer thickness and is particularly evident with a thicker oxide layer, which restricts the diffusion of PEDOT:PSS to Si. These micropores are estimated to be 16 μm in average diameter. The solar cell properties could be further improved by the use of surface-structured Si (pyramids or nanowires), addition of an appropriate solvent or surfactant in the PEDOT:PSS dispersion, and the use of better optimized electrode configurations (thickness, width, and spacing). The micropore defect formation in organic or polymer materials is difficult to observe using conventional cross-sectional microscopic techniques. The present 3D TOF-SIMS chemical imaging results

dx.doi.org/10.1021/ac401084x | *Anal. Chem.* 2013, 85, 6840−6845

therefore offer much needed new insights to complement existing conventional microscopic results. Moreover, the TOF-SIMS 3D chemical imaging technique could also be extended to investigate more complex systems (such as organic light-emitting diodes with multiple different layers), and these studies could lead to better understanding of the fundamental processes that occur at the intricate interface. The present 3D chemical imaging by TOF-SIMS technique could be further exploited to examine the interface of other systems, in order to optimize the processing parameters for even better solar cell performance.

■ ASSOCIATED CONTENT

Supporting Information

Additional information and figures as noted in text. This material is available free of charge via the Internet at http://pubs.acs.org.

■ AUTHOR INFORMATION

Corresponding Author

*E-mail: tong@uwaterloo.ca

Notes

The authors declare no competing financial interest.

■ ACKNOWLEDGMENTS

This work was supported by the Natural Sciences and Engineering Research Council of Canada.

■ REFERENCES

(1) Jeong, S.; Garnett, E. C.; Wang, S.; Yu, Z.; Fan, S.; Brongersma, M. L.; McGehee, M. D.; Cui, Y. *Nano Lett.* **2012**, *12*, 2971−2976.
(2) He, L.; Jiang, C.; Wang, H.; Lai, D.; Rusli. *Appl. Phys. Lett.* **2012**, *100*, 073503.
(3) Liu, Q.; Ono, M.; Tang, Z.; Ishikawa, R.; Ueno, K.; Shirai, H. *Appl. Phys. Lett.* **2012**, *100*, 183901.
(4) He, L.; Lai, D.; Wang, H.; Jiang, C.; Rusli. *Small* **2012**, *8*, 1664−1668.
(5) Ozdemir, B.; Kulakci, M.; Turan, R.; Unalan, H. E. *Appl. Phys. Lett.* **2013**, *99*, 113510.
(6) Shiu, S. C.; Chao, J. J.; Hung, S. C.; Yeh, C. L.; Lin, C. F. *Chem. Mater.* **2010**, *22*, 3108−3113.
(7) Woo, S.; Jeong, J. H.; Lyu, H. K.; Jeong, S.; Sim, J. H.; Kim, W. H.; Han, Y. S.; Kim, Y. *Physica B* **2012**, *407*, 3059−3062.
(8) Zhang, F.; Sun, B.; Song, T.; Zhu, X.; Lee, S. *Chem. Mater.* **2011**, *23*, 2084−2090.
(9) Lu, W.; Wang, C.; Yue, W.; Chen, L. *Nanoscale* **2011**, *3*, 3631−3634.
(10) Chen, T. G.; Huang, B. Y.; Chen, E. C.; Yu, P.; Meng, H. F. *Appl. Phys. Lett.* **2012**, *101*, 033301.
(11) Nasybulin, E.; Wei, S.; Kymissis, I.; Levon, K. *Electrochim. Acta* **2012**, *78*, 638−643.
(12) Fan, B.; Xia, Y.; Ouyang, J. *Proc. SPIE* **2009**, *7415*, 74151Q1−74151Q9.
(13) Fang, G.; Wu, S.; Xie, Z.; Geng, Y.; Wang, L. *Macromol. Chem. Phys.* **2011**, *212*, 1846−1851.
(14) Seeley, E. H.; Caprioli, R. M. *Anal. Chem.* **2012**, *84*, 2105−2110.
(15) Ren, X.; Weng, L. T.; Chan, C. M.; Ng, K. M. *Anal. Chem.* **2012**, *84*, 8497−8504.
(16) Jung, S.; Foston, M.; Kalluri, U. C.; Tuskan, G. A.; Ragauskas, A. J. *Angew. Chem., Int. Ed.* **2012**, *51*, 12005−12008.
(17) Yu, B.; Lin, W.; Wang, W.; Iida, S.; Chen, S.; Liu, K. C.; Kuo, C.; Lee, S.; Kao, W.; Yen, G.; You, Y.; Liu, C.; Jou, J.; Shyue, J. J. *ACS Nano* **2010**, *4*, 833−840.
(18) Fletcher, J. S.; Vickerman, J. C. *Anal. Chem.* **2013**, *85*, 610−639.
(19) Brown, A.; Vickerman, J. C. *Analyst* **1984**, *109*, 851−857.
(20) Muramoto, S.; Brison, J.; Castner, D. G. *Anal. Chem.* **2012**, *84*, 365−372.
(21) Pacholski, M. L.; Winograd, N. *Chem. Rev.* **1999**, *99*, 2977−3006.
(22) Kollmer, F. *Appl. Surf. Sci.* **2004**, *231−232*, 153−158.
(23) Kotter, F.; Benninghoven, A. *Appl. Surf. Sci.* **1998**, *133*, 47−57.
(24) Mahoney, C. M. *Mass Spectrom. Rev.* **2010**, *29*, 247−293.
(25) Mao, D.; Wucher, A.; Brenes, D. A; Lu, C.; Winograd, N. *Anal. Chem.* **2012**, *84*, 3981−3989.
(26) Rabbani, S.; Barber, A. M.; Fletcher, J. S.; Lockyer, N. P.; Vickerman, J. C. *Anal. Chem.* **2011**, *83*, 3793−3800.
(27) Lee, J. L. S.; Ninomiya, S.; Matsuo, J.; Gilmore, I. S.; Seah, M. P.; Shard, A. G. *Anal. Chem.* **2010**, *82*, 98−105.
(28) Shard, A. G.; Havelund, R.; Seah, M. P.; Spencer, S. J.; Gilmore, I. S.; Winograd, N.; Mao, D.; Miyayama, T.; Niehuis, E.; Rading, D.; Moellers, R. *Anal. Chem.* **2012**, *84*, 7865−7873.
(29) Restrepo, O. A.; Delcorte, A. *J. Phys. Chem. C* **2013**, *117*, 1189−1196.
(30) Uchic, M. D.; Groeber, M. A.; Dimiduk, D. M.; Simmons, J. P. *Scr. Mater.* **2006**, *55*, 23−28.